Berndt, E. B, B. T. Zavodsky, A. L., G. J. Jedlovec, N. J. Elmer, 2013: Impact of the Assimilation of Hyperspectral Infrared Profiles on Advanced Weather and Research Model Simulations of a Non-Convective Wind Event. Extended Abstract, *38th Natl. Wea. Assoc. Annual Meeting*, Charleston, SC, P2.7.

P2.7 Impact of the Assimilation of Hyperspectral Infrared Profiles on Advanced Weather and Research Model Simulations of a Non-Convective Wind Event

EMILY B. BERNDT[1], BRADLEY T. ZAVODSKY[2],
GARY J. JEDLOVEC[2], NICHOLAS J. ELMER[3]

[1]NASA Postdoctoral Program Marshall Space Flight Center, Huntsville, Alabama
[2]Short-term Prediction Research and Transition Center NASA/MSFC, Huntsville, Alabama
[3]University of Alabama in Huntsville, Huntsville, Alabama

ABSTRACT

Non-convective wind events commonly occur with passing extratropical cyclones and have significant societal and economic impacts. Since non-convective winds often occur in the absence of specific phenomena such as a thunderstorm, tornado, or hurricane, the public are less likely to heed high wind warnings and continue daily activities. Thus non-convective wind events result in as many fatalities as straight line thunderstorm winds. One physical explanation for non-convective winds includes tropopause folds. Improved model representation of stratospheric air and associated non-convective wind events could improve non-convective wind forecasts and associated warnings. In recent years, satellite data assimilation has improved skill in forecasting extratropical cyclones; however errors still remain in forecasting the position and strength of extratropical cyclones as well as the tropopause folding process. The goal of this study is to determine the impact of assimilating satellite temperature and moisture retrieved profiles from hyperspectral infrared (IR) sounders (i.e. Atmospheric Infrared Sounder (AIRS), Cross-track Infrared and Microwave Sounding Suite (CrIMSS), and Infrared Atmospheric Sounding Interferometer (IASI)) on the model representation of the tropopause fold and an associated high wind event that impacted the Northeast United States on 09 February 2013. Model simulations using the Advanced Research Weather Research and Forecasting Model (ARW) were conducted on a 12-km grid with cycled data assimilation mimicking the operational North American Model (NAM). The results from the satellite assimilation run are compared to a control experiment (without hyperspectral IR retrievals), North American Regional Reanalysis (NARR) reanalysis, and Rapid Refresh analyses.

1. Introduction

Rapidly intensifying cyclones are commonly associated with tropopause folds, which are identified by the presence of warm, dry, high-potential vorticity, ozone-rich stratospheric air (Danielson 1968). Tropopause folds are one explanation for damaging non-convective wind events. (Knox et al. 2011). Since non-convective winds are not associated with a specific phenomenon such as a tornado, thunderstorm, or hurricane, they are less likely to be taken seriously by the public; therefore, high wind warnings are often ignored. Therefore people tend to continue daily activities and non-convective winds cause as many fatalities as thunderstorm straight-line winds each year

Corresponding author address: Dr. Emily. B. Berndt, NASA Postdoctoral Program Fellow Marshall Space Flight Center, 320 Sparkman Drive, Huntsville, AL 35805
E-mail: emily.b.berndt@nasa.gov

(Ashley and Black 2008). Improved model representation of stratospheric air and associated non-convective wind events could improve non-convective wind forecasts and associated high wind warnings.

In recent years, satellite data assimilation has improved skill in forecasting extratropical cyclones; however, errors still remain in forecasting the position and strength of extratropical cyclones as well as the tropopause folding process. Since the tropopause folding process can be identified by model potential vorticity fields, and potential vorticity is defined at the product of absolute vorticity and static stability, could better representation of the temperature and moisture characteristics of stratospheric air improve model representation of tropopause folding and associated high winds? Von Ahn et al. (2005) note that predicting the timing of damaging hurricane-force wind associated with marine extratropical cyclones can be difficult since the storm may last on average 5 days, but high winds may only occur over a 24-hour period.

Since, abrupt folding of the tropopause is associated with a potential vorticity anomaly; approximately 1.5 to 2.0 potential vorticity units (PVU) mark the location of the dynamic tropopause (Thorncroft et al. 1993). Regions of stratospheric air and tropopause folds can be identified on a vertical cross section, similar to the schematic of a tropopause fold in Danielson (1968) Fig. 14. The goal of this study is to assess the impact of assimilating Hyperspectral Infrared (IR) sounders from Atmospheric Infrared Sounder (AIRS), Infrared Atmospheric Sounding Interferometer (IASI), and Cross-track Infrared and Microwave Sounding Suite (CrIMSS) on forecasting stratospheric air and tropopause folding.

2. Background on data assimilation

Currently, AIRS and IASI radiances are assimilated in the operational North American Model (NAM). Cloud clearing, error checking, and data thinning limit the number of radiances assimilated. For example a 281-channel subset of the full 2378 AIRS channels are assimilated and only 200 carefully chosen IASI channels are assimilated (Le Marshall et al. 2006; Hilton et al. 2012). Spectral and spatial data thinning techniques translate to data assimilation of less than 1% of the total AIRS volume (Goldberg et al. 2003). Radiance data contain limited information about the vertical temperature and moisture structure of the atmosphere and are restricted to cloud-free fields of view. Advanced schemes are under development to utilize cloud-affected radiances; however, advanced schemes can be computationally expensive and significant progress depends on developments in data assimilation, radiative transfer models, and numerical models (Hilton et al. 2012). The advantage of Hyperspectral IR profiles is that they can be assimilated in some partly cloudy scenes and can be assimilated as radiosonde observations (RAOB) without the use of a computationally expensive radiative transfer model such as the CRTM (Community Radiative Transfer Model). The only caveat is that in such a process the profiles are assigned the same error as the ROABs, which is not entirely ideal.

3. Experiment setup

The Developmental Testbed Center (DTC) Gridpoint Statistical Interpolation (GSI) version 3.0 and Advanced Research Weather Research and Forecasting (ARW; Skamarock et al. 2007) Model version 3.3 were used for cycled data assimilation and 48-hour model forecasts. Forecast cycling mimicked the operational NAM where observations were assimilated at 3-hour intervals starting at 12

hours before the forecast initialization time (Fig. 1). Observational data were obtained in 3-hour intervals and span a time period of +/- 1.5 hours centered on the cycle time. Each cycle was assigned a "time-minus" (tm) annotation to describe the time before the forecast in which the observations were assimilated (eg. tm12, tm09, tm06, tm03, tm00). The cycling methodology allows for satellite data not available in real-time to be incorporated in the data assimilation.

The model was initialized with Global Forecast System (GFS) model data on a 12-km domain with 35 vertical levels. The scheme choices were the same as the operational National Severe Storms Laboratory (NSSL) Weather Research and Forecasting (WRF) model. A control simulation was conducted with data assimilation similar to operations which includes conventional observations in NCEP prepbufr files and satellite observations listed in Table 1. The experiment simulation assimilated the same observations as the control run but additionally assimilated the AIRS, IASI, and CrIMSS temperature (T) and moisture (q) profiles. Note the AIRS, IASI, and CrIMSS radiances were not assimilated into the control or experiment simulations to isolate the impacts of Hyperspectral IR profiles assimilation from those same instruments. The Hyperspectral IR profiles were processed and appended to the prepbufr files and assigned the same error as conventional RAOBs.

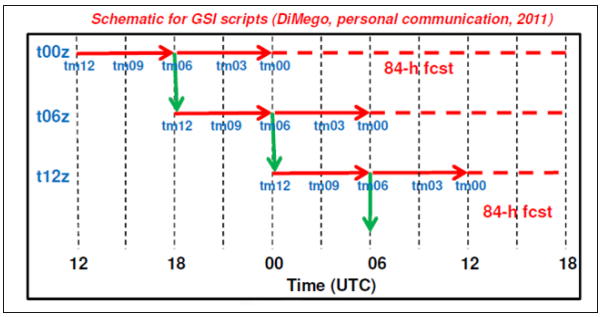

Figure 1. Schematic for forecast cycling and data assimilation with SPoRT scripts that run GSI and ARW.

Table 1. Satellite and conventional observations assimilated in control and experiment.

Type	Control	Experiment
AMSU-A	N15, N18, N19, MetOp-A, Aqua	N15, N18, N19, MetOp-A, Aqua
MHS	N18, N19, MetOp-A	N18, N19, MetOp-A
HIRS	N17, N19, MetOp-A	N17, N19, MetOp-A
Sounder	GOES13, GOES15	GOES13, GOES15
AIRS, IASI, CrIMSS		L2 T and q profiles
Conventional	Soundes, Aircraft, SatWinds, RadWinds, GPSRO, METAR,BUOY	Soundes, Aircraft, SatWinds, RadWinds, GPSRO, METAR,BUOY

3. Experiment analysis

a. GSI performance

Figure 2 through Fig. 6 show the locations and innovations of Hyperspectral IR profiles assimilated at 300 hPa during the tm12 to tm00 GSI cycles for the 0000 UTC 09 February 2013 experimental model run. The greatest number of profiles were assimilated during the tm09, tm06, and tm00 GSI cycles due to the correlation of satellite orbit tracks with the model domain. Innovations, which represent the analysis minus the background, for the experiment simulation show yellow/red (green/blue) locations where the individual

profiles increased (decreased) the temperature analysis field. During the tm06 GSI cycle, some profiles had a positive impact on the model temperature analysis field surrounding the region of interest (Fig. 4). Any missing profile locations within a swath are due to the presence of thick clouds (i.e. Figs. 4 and 6). Thick clouds limited the number of profiles assimilated over the region of interest during the tm00 cycle.

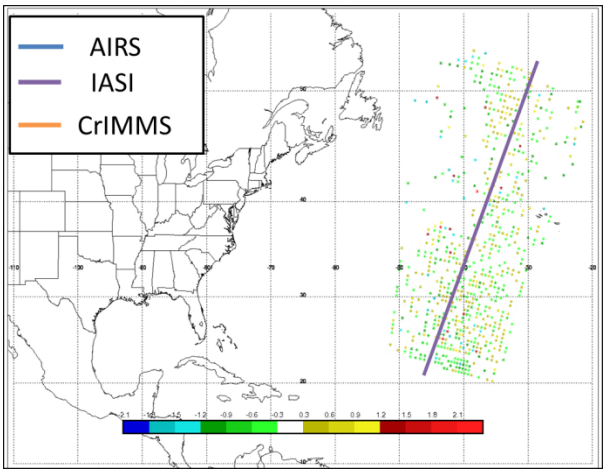

Figure 2. 300 hPa Innovations for assimilated Hyperspectral IR profiles at cycle tm12 from 0000 UTC 09 Feb 2013 (valid 1200 UTC 08 Feb 2013).

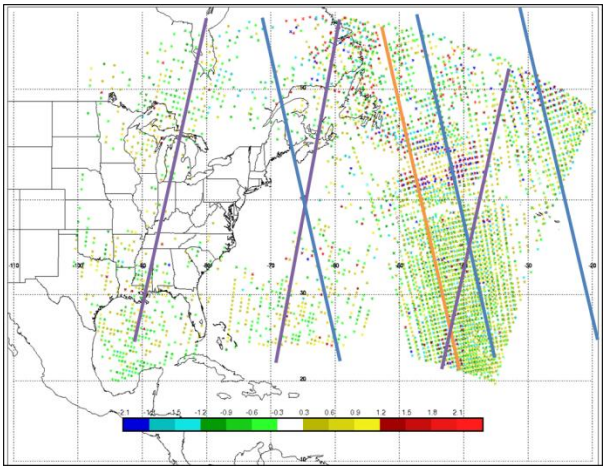

Figure 3. 300 hPa Innovations for assimilated Hyperspectral IR profiles at cycle tm09 from 0000 UTC 09 Feb 2013 (valid 1500 UTC 08 Feb 2013).

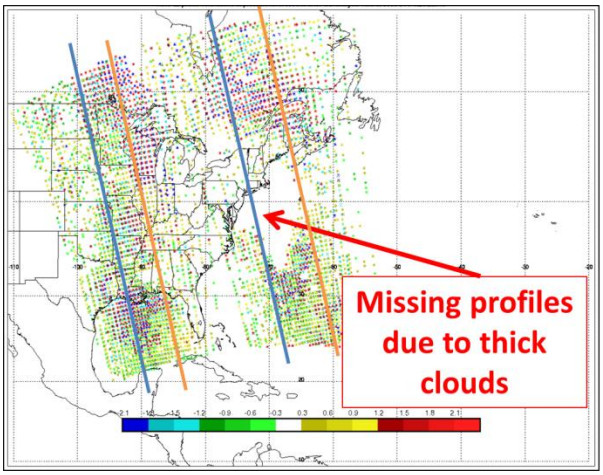

Figure 4. 300 hPa Innovations for assimilated Hyperspectral IR profiles at cycle tm06 from 0000 UTC 09 Feb 2013 (valid 1500 UTC 08 Feb 2013).

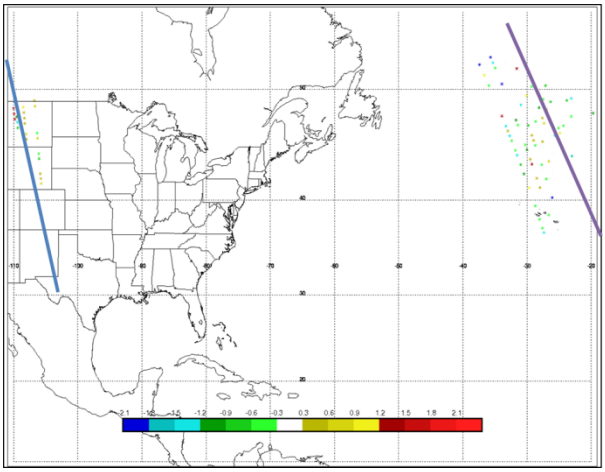

Figure 5. 300 hPa Innovations for assimilated Hyperspectral IR profiles at cycle tm03 from 0000 UTC 09 Feb 2013 (valid 1500 UTC 08 Feb 2013).

The 300 hPa temperature analysis increment shows the impact of assimilating the Hyperspectral IR profiles (Fig. 7). The analysis increment is calculated by the difference of the experiment analysis and control analysis. Even though there were missing profiles during the tm00 GSI cycle over the region of interest (circled in Fig. 7), the cumulative effect of data assimilation cycling still provided information to update the final temperature analysis field for the 0000 UTC 09 February 48-hour forecast.

Compared to the temperature analysis increment, the moisture analysis increment impacted the lower-levels to a greater degree; due to this fact the 300 hPa moisture analysis increment is not shown.

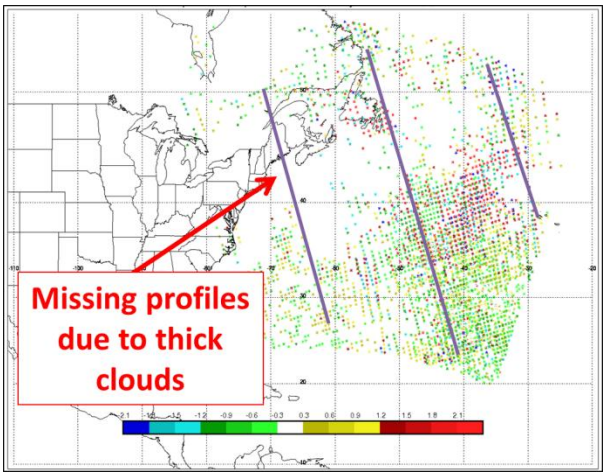

Figure 6. 300 hPa Innovations for assimilated Hyperspectral IR profiles at cycle tm00 from 0000 UTC 09 Feb 2013 (valid 1500 UTC 08 Feb 2013).

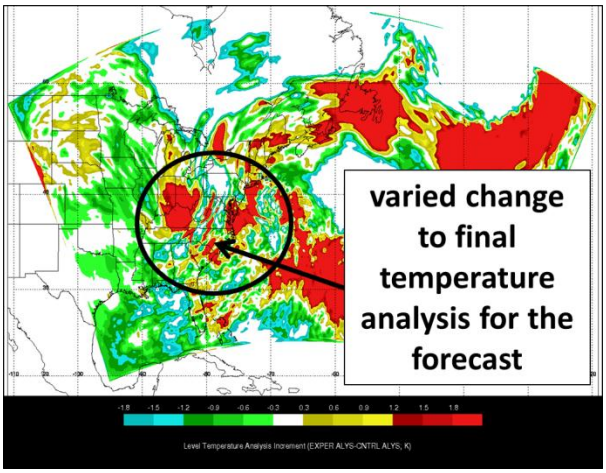

Figure 7. 300 hPa Temperature Analysis Increment of Experiment minus Control during cycle tm00 for 0000 UTC 09 February 2013 simulations.

b. Forecast impact

Comparison of reanalysis data, simulated model fields, and difference fields between the experiment and control show the impact of assimilating the Hyperspectral IR profiles on the model output. Inspection of NARR tropopause height and temperature (Fig. 8) reveals warm stratospheric air and low tropopause height located over the region of interest. Upon comparing the control and experiment temperature and height fields, there are only subtle visual differences. The tropopause temperature difference plot shows the control overestimated the tropopause temperature in the region of stratospheric air. There are only subtle differences in the tropopause temperature. Moisture profiles had little impact in, dry upper-level regions and more impact in the lower levels (Fig. 9). The tropopause fold in the control run had a different shape than the NARR data; however, the experiment more closely resembled the shape of the tropopause fold. Even though the shape was similar, the experiment overestimated the magnitude of the potential vorticity anomaly. Analysis of the near-surface wind field showed strong cold conveyor belt winds that wrapped around the north side of the low pressure center and a region of non-convective winds south of the low pressure center. The magnitude of the experiment winds were closer to the NARR analysis, but the location was displaced.

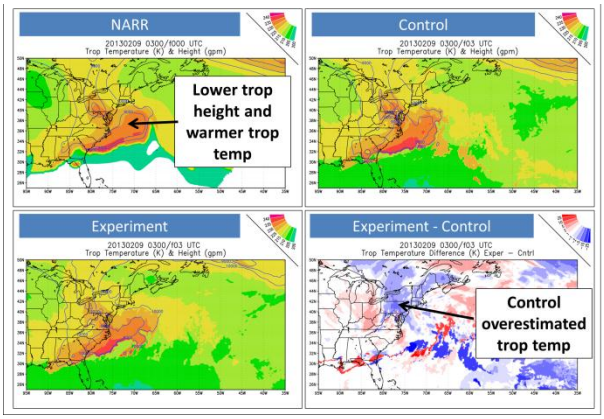

Figure 8. 0300 UTC 09 February 2013 Troposphere temperature (K) and height (gpm, blue contours) Upper Left: NARR; Upper Right: 3-hr forecast from 0000 UTC 09 February 2013 Control Simulation, Lower Left: 3-hr forecast from 0000 UTC 09 February 2013 Experiment Simulation, Lower Right: Tropopause

temperature difference (K) for Experiment minus Control.

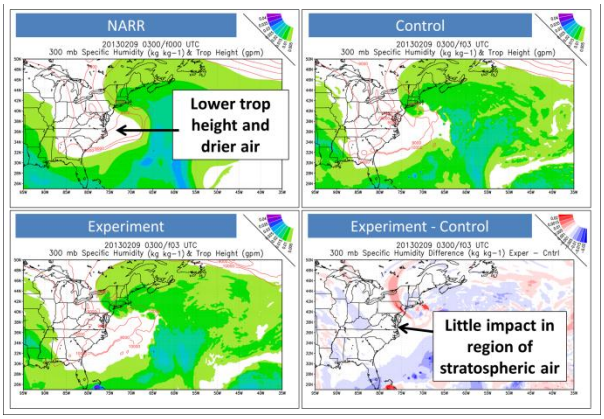

Figure 10. 0300 UTC 09 February 2013 Potential Vorticity (K m^2/kg/s) and wind (m/s, barbs) Upper Left: NARR, Upper Right: 3-hr forecast from 0000 UTC 09 February 2013 Control Simulation, Lower Left: : 3-hr forecast from 0000 UTC 09 February 2013 Experiment Simulation, Lower Right: Potential Vorticity difference (K m^2/kg/s) from Experiment minus Control.

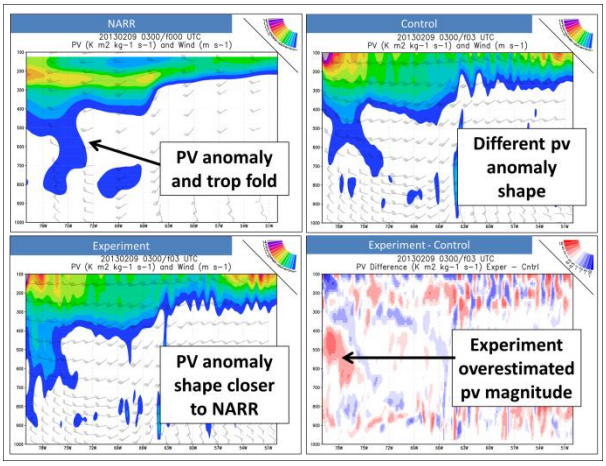

Figure 9. 0300 UTC 09 February 2013 300 hPa Specific Humidity (kg/kg, shaded) and tropopause height (gpm, red contours) Upper Left: NARR, Upper Right: 3-hr forecast from 0000 UTC 09 February 2013 Control Simulation, Lower Left: : 3-hr forecast from 0000 UTC 09 February 2013 Experiment Simulation, Lower Right: 300 hPa Specific humidity difference (kg/kg) for Experiment minus Control.

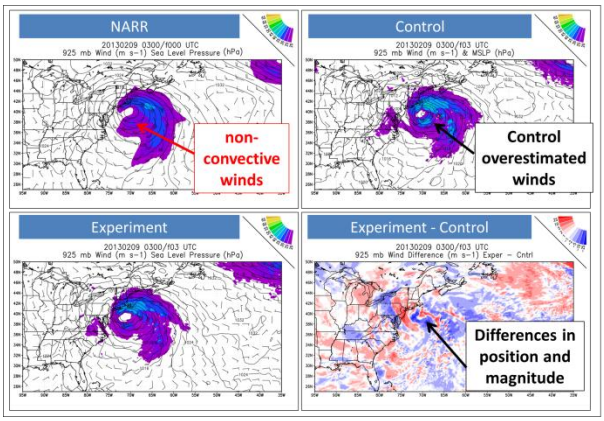

Figure 11. 0300 UTC 09 February 2013 925 hPa wind (m/s, shaded and barbs) and sea level pressure (hPa) Upper Left: NARR; Upper Right: 3-hr forecast from 0000 UTC 09 February 2013 Control Simulation; Lower Left: : 3-hr forecast from 0000 UTC 09 February 2013 Experiment Simulation; Lower Right: 925 hPa wind difference (m/s) for Experiment minus Control.

4. Conclusions

Assimilation of AIRS, IASI, and CrIMSS Hyperspectral IR profiles resulted in analysis increments of greater than +/-3°C in regions surrounding the thick clouds associated with the storm system of interest. Overall, the assimilation of Hyperspectral IR profiles improved the representation of temperature characteristics of stratospheric air and the shape of the tropopause fold, but had little impact on moisture characteristics in upper-level dry regions. Since changes in the near-surface wind field may be related to assimilation of temperature and moisture at low levels, an experiment that only assimilates upper level profiles will isolate whether changes to the upper-level representation of stratospheric air change the near-surface wind field.

Acknowledgements. This research was supported by an appointment to the NASA Postdoctoral Program at Marshall Space Flight Center, administered by Oak Ridge Associated Universities through a contract with NASA. MERRA data were acquired

from the Global Modeling and Assimilation Office (GMAO) and the Goddard Earth Sciences Data and Information Services Center (GES DISC). RAP data were obtained from the Atmospheric Radiation Measurement Program sponsored by the U.S. Department of Energy, Office of Science, Office of Biological and Environmental Research, Climate and Environmental Sciences Division. Dataset was originally produced at NOAA's National Center for Atmospheric Prediction (NCEP) and is available in original grib format through NOAA NCDC's access page. It is also available in the same format from NCARNORTH AMERICAN REGIONAL REANALYSIS: A long-term, consistent, high-resolution climate dataset for the North American domain, as a major improvement upon the earlier global reanalysis datasets in both resolution and accuracy, Fedor Mesinger et. al, submitted to BAMS 2004.

REFERENCES

Ashley, W. S. and A. W. Black 2008: Fatalities Associated with Nonconvective High-Wind Events in the United States. *Journal of Applied Meteorology and Climatology* 47, pp. 717-725.

Browning, K.A., 2004: The Sting at the End of the Tail: Damaging Winds Associated with Extratropical Cyclones. *Q. J. R. Meteorol. Soc.*, 130, 597, pp. 375-399.

Clark, P. A., K. A. Browning, and C. Wang, 2005: The sting at the end of the tail: Model diagnostics of fine-scale three-dimensional structure of the cloud head. *Q. J. R. Meteorol. Soc.*, 131, 610, pp. 2263-2292.

Danielson, E. F., 1968: Stratospheric-tropospheric exchange based on radioactivity, ozone, and potential vorticity. *J. Atmos. Sci.*, 25, 502-518.

Knox, J. A., J. D. Frye, J. D. Durkee, and C. M. Fuhrmann, 2011: Non-Convective High Winds Associated with Extratropical Cyclones. *Geography Compass*, Vol. 5, Issue 2, 63-89.

Martínez-Alvarado, O., F. Weidle, and S. L. Gray, 2010: Sting Jets in Simulations of a Real Cyclone by Two Mesoscale Models. *Mon. Wea. Rev.*, 138, 4054–4075.

Martínez-Alvarado, O., S. L., J. L. Catto, and P. A. Clark, 2012: Sting Jets in Intense winter North-Atlantic Windstorms. *Environ. Res. Lett.*, **7**.

Schultz, D., D. Keyser, and L. F. Bosart, 1998: *The Effect of Large-Scale Flow on Low-Level Frontal Structure and Evolution in Midlatitude Cyclones. Mon. Wea. Rev.*, **126**, 1767-1791.

Schultz, D., and J. Sienkiewicz, 2013: Using Frontogenesis to Identify Sting Jets in Extratropical Cyclones. *Wea. Forecasting*. **28**, 603-613.

Shapiro, M. A. and D. Keyser, 1990: Fronts, jet streams and the tropopause. *Extratropical Cyclones, The Erik Palmén Memorial Volume*, C. W. Newton and E. O. Holopainen, Eds., Amer. Meteor. Soc., 167-191.

Thorncroft, C. D., B. J. Hoskins, and M. E. McIntyre, 1993: Two paradigms of baroclinic-wave life-cycle behavior. *Quart. J. Roy. Meteor. Soc.*, **119**, 17-55.

Van Haver, P. and Coauthors, 1996: Climatology of tropopause folds at midlatitudes. *Geophys. Res. Lett.*, 23, 1033-1036.

Zavodsky B.T., A. L. Molthan, and M.J. Folmer, 2013: Multispectral Imagery for Detecting Stratospheric Air Intrusions Associated with Mid-Latitude Cyclones. Journal of Operational Meteorology, 1 (7), 71-83.

Ziemke J. R., S. Chandra, G. J. Labow, P. K. Bhartia, L. Froidevaux, J. C. Witte, 2011: A global climatology of tropospheric and stratospheric ozone derived from Aura OMI and MLS measurements. *Atmospheric Chemistry and Physics*, 11, 9237-9251.